

http://pubs.acs.org/journal/aesccq Article

Chlorine-Initiated Oxidation of α -Pinene: Formation of Secondary Organic Aerosol and Highly Oxygenated Organic Molecules

Catherine G. Masoud and Lea Hildebrandt Ruiz*



Cite This: ACS Earth Space Chem. 2021, 5, 2307-2319



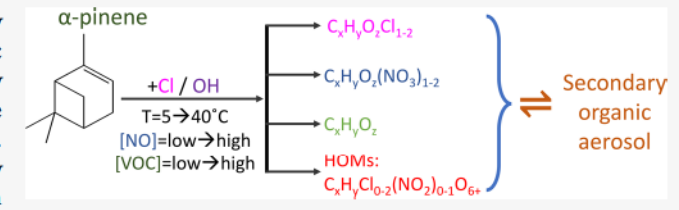
ACCESS I

Metrics & More

Article Recommendations

Supporting Information

ABSTRACT: The oxidation of α -pinene, the most abundantly emitted monoterpene, is an important source of secondary organic aerosol. Previous work has focused on α -pinene oxidation by hydroxyl (OH) radicals or ozone (O₃), yet the effect of chlorine radicals (Cl) as oxidizing agents has not received much attention. Recent ambient measurements suggest that Cl could substantially affect SOA formation in continental as well as coastal regions. In this work, we conducted environmental chamber experiments on



the Cl-initiated photo-oxidation of α -pinene leading to the formation of oxidized products including highly oxygenated organic molecules (HOM) and SOA. We use a Filter Inlet for Gases and Aerosols mounted onto a High-Resolution Time-of-Flight Chemical Ionization Mass Spectrometer (FIGAERO-CIMS) to monitor gas- and particle-phase products and to investigate their gas-particle partitioning. We identify over 600 species including 197 chlorinated and nonchlorinated HOM, which are up to six times more abundant in the particle phase than in the gas phase. We also find that SOA yields are enhanced under low NO_x conditions. Overall, our work suggests that chlorine-initiated oxidation of α -pinene can substantially impact tropospheric SOA formation given the fast chlorine chemistry and the formation of low volatility HOM which contribute to high SOA yields.

KEYWORDS: Highly oxygenated organic molecules, secondary organic aerosol, chlorine chemistry, α -pinene, photooxidation

1. INTRODUCTION

Fine particulate matter (particles with a diameter of 2.5 μ m or less – PM_{2.5}) are known to have negative impacts on human health ^{1–4} and an uncertain but considerable effect on climate forcing. ⁵ Organic aerosol (OA) accounts for 20–90% of the fine particulate mass and can be primary or secondary in nature. Secondary organic aerosol (SOA) forms from the oxidation of volatile organic compounds, leading to the formation of lower vapor pressure species that can partition to the aerosol phase. SOA comprises 50–85% of the global OA budget. ⁶ Up to 42% of OA in the southeastern United States was recently attributed to monoterpene-derived SOA. ⁷ The most abundantly emitted monoterpene in the atmosphere is α -pinene; ⁸ thus, understanding α -pinene oxidation and resulting formation of SOA is important to understanding atmospheric OA budgets. ^{7,9}

For decades, researchers have focused on the oxidation of volatile organic compounds (VOCs) with the most reactive and abundant oxidants in the atmosphere - hydroxyl radicals (OH·), ozone (O₃), and nitrate radicals (NO₃·), and the ensuing formation of SOA from these reactions. However, not much attention has been directed to studying chlorine radicals (Cl·) as oxidants actively participating in the atmospheric oxidation of VOCs and formation of SOA. This is mainly due to the long-held belief that chlorine chemistry is only relevant in coastal areas where NaCl is a significant Cl source. However, recent measurements of reactive chlorine species in inland

regions have shown that their concentrations are higher than previously anticipated. $^{10-12}$ Moreover, laboratory studies have shown the importance of halogen (Cl) chemistry in SOA formation from various VOC precursors including common monoterpenes (\$\alpha\$-pinene, \$\beta\$-pinene, and \$d\$-limonene), 13 isoprene, 14 toluene, 15,16 and a number of alkanes. 17,18 While concentrations of Cl atoms are expected to be lower than the concentrations of OH in most environments, Cl-initiated oxidation can compete with OH-initiated oxidation in the presence of Cl atoms due to faster reaction rates. The rate constant for the reaction of Cl radicals with most atmospherically relevant VOCs is up to 2 orders of magnitude higher than the rate constant of the OH-initiated oxidation. 19,20 In the case of \$\alpha\$-pinene, the rate constant for Cl-initiated oxidation is about ten times faster (5 × 10^{-10} cm^3 molecule $^{-1}$ s $^{-1}$) than the rate constant for OH-initiated oxidation (5 × 10^{-11} cm^3 molecule $^{-1}$ s $^{-1}$). $^{19-21}$

A chlorine atom can initiate the oxidation of α -pinene by abstracting a hydrogen atom or by adding to a double bond, which results in the formation of an organochloride. ^{19,22–25}

Special Issue: Mario Molina Memorial

Received: May 20, 2021
Revised: August 6, 2021
Accepted: August 15, 2021
Published: September 2, 2021





Subsequent chemistry can result in loss of the Cl moiety, 13 and as such, it is challenging to determine which of these pathways is dominant. Finlayson-Pitts et al. 19 suggest that for large biogenic compounds (such as $C_{10}H_{16}$), which contain a large number of abstractable hydrogen atoms, H-abstraction may be the primary oxidation mechanism. Cai and Griffin 13 suggest that even though H-abstraction may account for a significant fraction of the reaction between $C_{10}H_{16}$ and Cl, the dominant pathway is likely the Cl-addition pathway. Ofner et al. 26 provide evidence for both pathways but do not quantify the respective contributions to the overall reaction. Wang et al. 27 suggest that based on observed spectra of highly oxygenated organic molecules (HOM) from the α -pinene+Cl reaction, the H-abstraction pathway may be the dominant pathway for the formation of HOM; they do not discuss the overall dominant pathway.

Highly oxygenated organic molecules (HOM)²⁷ are known to contribute to the formation of new atmospheric particles^{28–32} and secondary organic aerosol^{32,33} due to their low volatility.³⁴ HOM form in the gas phase through autoxidation, where a peroxy radical (RO₂) undergoes an intramolecular hydrogen shift reaction forming a hydroperoxide group and an alkyl radical, to which molecular oxygen can then add to form a more highly oxidized peroxy radical.³⁴ HOM are identified based on their formation mechanism (autoxidation involving peroxy radicals) and the number of oxygen atoms in the compound (commonly six or more O atoms).³⁴ Nitrated HOM, which were recently observed over boreal regions, are defined as having at least eight oxygen atoms, as organonitrates can contain six to seven oxygen atoms without the involvement of peroxy radicals.³⁵

A few previous studies have examined SOA formation from the α -pinene+Cl reaction. Cai and Griffin¹³ investigated the SOA formation potential from reactions of α -pinene+Cl under low NOx conditions in the absence of inorganic seed and found SOA yields to be comparable to SOA yields from α pinene oxidation initiated by other common atmospheric oxidants such as O3 and NO3. They also suggested that the initial ratio of Cl₂/α-pinene could have an impact on SOA formation from this reaction. Ofner et al.26 combined an aerosol smog-chamber and aerosol flow-reactor to study halogenated organic aerosol formation from the α -pinene+Cl reaction using Fourier-transform infrared (FTIR) spectroscopy. They concluded that halogen-driven formation of secondary organic aerosol significantly influences physicochemical properties of SOA including water solubility, the potential to act as cloud condensation or ice nuclei, the adsorption of gas-phase species, and interaction with sunlight, all of which have implications to radiative forcing. Wang et al.²⁷ used an NO3-based Chemical Ionization-Atmospheric Pressure-interface Time of Flight mass spectrometer (CI-APi-LToF) to show that HOM formation is observable under low NO_x conditions at average molar yields of 1.8% when α -pinene +Cl react at atmospherically relevant conditions.

To the best of our knowledge, no work has previously reported the impact of temperature and NO_x conditions on SOA mass yields and gas- and particle-phase HOM for the α -pinene+Cl system. Given that chlorine chemistry is more important than previously thought in a variety of environments, it is essential to investigate the Cl-initiated oxidation of α -pinene under different conditions.

We conducted environmental chamber experiments on the Cl-initiated oxidation of α -pinene, focusing on the formation of

several gas and particle-phase products including HOM, organic nitrates, and SOA as a function of temperature, VOC precursor concentration, and NO_x concentration. A High-Resolution Time of Flight Chemical Ionization Mass Spectrometer (HR-ToF-CIMS) using iodide as reagent ion measured vapor phase products of the reaction, with the FIGAERO (Filter Inlet for Gases and Aerosols) providing insight into particle phase composition. The Aerosol Chemical Speciation Monitor (ACSM) provided bulk composition of particle-phase products, including insight into the extent of oxidation and formation of particulate nitrates. We compare results from these Cl-initiated oxidation experiments to results from OH-initiated experiments.

2. METHODOLOGY

2.1. Environmental Chamber and Instrumentation Overview. To study the formation of gas- and particle-phase products from Cl-initiated oxidation of α -pinene, we experimentally simulate the outdoor atmosphere in a controlled laboratory setting. A 10 m³ Teflon environmental chamber housed within a temperature-controlled room (Frost Environmental Rooms Inc.) is surrounded by sets of fluorescent UV-A lights, with peak emission at 368 nm, resulting in an NO₂ photolysis rate of 0.3 min⁻¹. The Teflon chamber is not actively stirred, but previous characterization of the chamber shows that concentrations of injected compounds stabilize within 15-20 min of injection. Before any photooxidation experiment is conducted, we use an AADCO clean air generation system to flush the chamber with clean (particle-, methane-, VOC-free) air at 100 L min-1 for ~14 h, resulting in a particle number concentration in the chamber of <10 cm⁻³. We fill the Teflon bag with clean humidified air. We use an Aerosol Generation System (Brechtel, AGS Model 2002) to inject neutral inorganic seed into the chamber using a 0.05-0.1 M solution of ammonium sulfate, (NH₄)₂SO₄. The seed aerosol provides surfaces for organic vapors to condense onto and form SOA once the photo-oxidation begins. We also use the inorganic seed as an inert tracer to facilitate wall loss correction. We use a mass flow controller to inject desired amounts of Cl2 gas (which forms Cl- upon photo-oxidation) from a Cl₂ cylinder (Airgas, 100 ppm in N₂). For high NO_x experiments, we use a mass flow controller to inject NO from a cylinder (Airgas, 10 ppm in N2). For experiments with OH radicals, we pass clean air through an H₂O₂ solution (30-40%, Fischer Scientific) for 1.5 h to send H₂O₂ vapors into the chamber.

We inject microliters of α -pinene (98%, Acros Organics) via a syringe mounted onto a heated glass bulb with 2.0 SLPM of clean air carrying the VOC into the chamber. We then wait for 30 min to ensure sufficient mixing of the reactants within the chamber. We then turn on the UV lights to initiate the photo-oxidation and leave the UV lights on for 60 min unless otherwise stated.

We conduct experiments at three different temperatures (5 °C, 25 °C, 40 °C) and at ~40% relative humidity, with one experiment carried out at dry conditions (RH < 5%) for comparison. We conduct "blank" or cleaning experiments before and after each photo-oxidation experiment in which we inject inorganic ammonium sulfate seed and Cl_2 gas into the chamber without addition of a VOC, and we keep the UV lights on for several hours to consume organic compounds that may be on the chamber walls or suspended within the chamber from previous experiments. Negligible organic aerosol is

Table 1. Summary of Experimental Conditions and Results

Exp. #	Experimental details	VOC ₀ ^a [ppb]	NO ₀ ^a [ppb]	Cl_{20}^a [ppb]	Temp [°C]	$SOA^b [\mu g m^{-3}]$	Y_{SOA}^{b}	f_{44}^{b}	f_{NO3}^{b}	HOM F _p ^e
1	Base case, RH < 5%	15	15	15	25	40	0.46	0.13	0.08	0.81
2	Base case	15	15	15	25	41	0.48	0.15	0.03	0.65
3	Low NO _x	15	0	15	25	73	0.85	0.10	0.03	0.80
4	$1/3 \times \text{precursor conc.}$	5	5	5	25	14	0.50	0.14	0.04	0.58
5	3 × precursor conc.	45	45	45	25	247	0.96	0.11	0.07	0.85
6^d	Base case	15	15	15	25	37	0.44	0.13	0.07	0.75
7^d	Low temperature ^c	15	15	15	5	94	1.09	0.08	0.08	0.85
8^d	High temperature	15	15	15	40	31	0.36	0.11	0.07	0.59
9^d	H_2O_2	30	0	0	25	73	N/A	0.08	0.02	0.81
10^d	$H_2O_2 + NO$	15	15	0	25	24	N/A	0.07	0.06	0.51

^aInitial concentrations. ^bReported at the maximum Org signal. ^cmax SOA observed at 57 min.; lights were turned off at 85 min. ^dExperiments conducted in a new Teflon chamber. ^cFraction of HOM in the particle phase.

produced in these experiments indicating that the chamber is clean.

A suite of instrumentation measuring gas- and particle-phase products surround and are continuously sampling from the chamber (simplified schematic shown in Figure S1). An Aerodyne Aerosol Chemical Speciation Monitor (ACSM, Aerodyne Research Inc.) measures particle-phase products speciated as organics, chlorides, nitrates, sulfates, and ammonium.³⁶ A Scanning Electrical Mobility Spectrometer (SEMS, Brechtel Model 2002) size-selects and counts particles, resulting in size distribution measurements of the aerosol. A Filter Inlet for Gases and Aerosols mounted onto a High-Resolution Time of Flight Chemical Ionization Mass Spectrometer (FIGAERO-CIMS, Aerodyne Research Inc.) provides high resolution information on the chemical composition of the evolving gas- and particle-phase products;³⁷⁻⁴⁰ these measurements are discussed in more detail below. A cavity attenuated phase shift NO2 analyzer (CAPS-NO2, Environnement S.A AS32M), a chemiluminescence NO/ NO, analyzer (Teledyne Model 200E), a photometric ozone analyzer (Teledyne Model 400E), and temperature and RH probes record relevant trace gas concentrations and experimental conditions throughout the experiment.

Experiments presented in this work were conducted in two different Teflon chambers. The chamber used for the first few experiments (E1–E5 from Table 1) was ~3 years old, whereas the one used for the later experiments (E6–E10 from Table 1) was a few months old when the experiments were conducted. After replacing the chamber, we conducted multiple conditioning experiments (photooxidation in the presence of seed aerosol leading to formation of OA) until we clearly observed repeatability between experiments, suggesting that wall losses were the same and reproducible.

2.2. FIGAERO-CIMS Operation and Data Analysis. The FIGAERO-CIMS records gas-phase data at a 1 Hz time resolution and particle phase data at 1-1.5 h time resolution. Iodide (I⁻) as chemical reagent is sensitive toward slightly to highly oxidized, chlorinated, and nitrogenated species. The FIGAERO inlet has been described in detail elsewhere. Briefly, the FIGAERO-CIMS alternates between two operational modes: in the gas sampling and aerosol collection mode, vapors are sampled and detected in real time, while the gas—aerosol mixture is collected onto a PTFE filter (Zefluor 2.0 μ m 24 mm, Pall Corp.) in preparation for desorption. In the particle desorption mode, heated N₂ gas is passed through the filter volatilizing the collected particles, and the vapor (volatilized particles) is analyzed with the CIMS.

For these experiments, we collect particles onto the PTFE filter after the UV lights are turned off halting most of the gasphase chemistry, and the products have had a chance to equilibrate within the chamber. We collect the aerosol for different time periods (15-45 min), with 45 min of particle desorption between collection periods. During particle desorption, heated ultra-high-purity nitrogen (UHP N₂) gas is passed through the filter using a temperature-programmed ramp. The temperature ramp includes 1 min of room temperature (25 °C) desorption to minimize any contribution from adsorbed vapor-phase compounds, 20 min of thermal ramping from 25 to 200 °C, 10 min of "filter-baking" at 200 °C to remove low-volatility material from the filter, followed by a cool-down period of 14 min back to 25 °C. The thermal desorption behavior of different compounds provides insight into their volatility, as more volatile compounds are expected to desorb from the filter at lower temperatures. 40,43-45

We analyze the FIGAERO-CIMS data in Igor Pro v 6.3 using the instrument analysis software Tofware v 2.5.11. The mass-to-charge calibration is based on three calibrants: I, $I(H_2O)^-$, and I_3^- covering a mass-to-charge range from 127 to 381 m/z and is fit to a two-parameter model with accuracy within 3 ppm. We perform high-resolution (HR) peak fitting by first conducting a targeted search of compounds that are known products of the α -pinene + Cl, 13 α -pinene + OH, 46,47 and α -pinene + O₃ reactions. We then fit additional compounds based on their exact m/z. When there are two possible molecular formulas (with similar m/z) that can be fit, where one is a closed-shell compound and the other is a radical, we choose the closed-shell compound, as it is more likely to be measured by the instrument. After obtaining the high-resolution time-series of the fitted peaks, we normalize the signals by the reagent ion (I-), and then multiply each signal by a reference value of $I^- = 10^6$ ions s⁻¹.

To study the effect of various experimental conditions on HOM formation, we follow the formation of HOM in the gas and particle-phases for Cl- and OH-initiated oxidation experiments. We define HOM in this work as C_9-C_{10} (monomeric) compounds containing six or more oxygen atoms³⁴ (eight or more oxygen atoms for nitrated HOM³⁵). For each phase, we calculate the total HOM signal (ions/second or counts/second, cps) and use the ratio of these signals (particle/gas signal) to gain insight into their gas—particle partitioning.

We assume complete consumption of α -pinene in Clinitiated experiments (experiments 1–8), which is consistent with chamber modeling (see section S.7 in the Supporting

Information) that suggests α -pinene consumption within 10 min, and with the peak concentrations of organic aerosol occurring within \sim 20 min of the experiment (with UV lights on for 60 min).

We convert the gas-phase signal units from ions/s to ions/volume using the sampling rate of the ToF-CIMS (2 LPM) to enable a direct comparison of gas and particle phase signals. We integrate the desorption signal for the particle phase (ions/s) with respect to desorption time (s) to obtain a total particle phase signal (ions). We convert the total particle phase signal (ions) to the equivalent value in ions/vol using the particle collection rate and the collection time. The equations we use to convert the gas and particle signals to equivalent values are as follows:

$$\begin{aligned} \text{Particle signal} & \left[\frac{\text{ions}}{\text{vol}} \right] = \\ & \underline{\qquad \qquad \qquad } \\ & \underline{\qquad \qquad } \\ & \text{Particle collection period [min]} \times \text{Particle collection rate} \left[\frac{\text{L}}{\text{min}} \right] \end{aligned}$$

$$Gas signal \left[\frac{ions}{vol} \right] = \frac{Average signal \left[\frac{ions}{sec} \right]}{CIMS sampling rate \left[\frac{2 L}{min} \right] \times \left[\frac{1}{60} \frac{min}{sec} \right]}$$
(2)

We use FIGAERO-CIMS data to create two-dimensional thermograms for the experiments in this work which provide insight into SOA volatility. ¹⁷ Briefly, we compile one-dimensional plots of particle signal normalized to its maximum value versus desorption temperature (°C) at each m/z, into one two-dimensional thermogram where the y-axis is the unit m/z, the x-axis is desorption temperature, and the color within the plot indicates normalized signal intensity.

2.3. ACSM Operation and Data Analysis. We measure bulk chemical composition of the submicron, nonrefractory species using the Aerosol Chemical Speciation Monitor³⁶ at 1 min intervals. In the ACSM, particles are flash-vaporized at 600 °C, and the resulting vapors are ionized via electron impact ionization (EI). Ions between m/z 10 and 150 are then detected at unit mass resolution by a quadruple mass spectrometer at a scan speed of 200 ms amu-1. The ACSM alternates measurements of filtered ("open") and unfiltered ("closed") mass spectra to give background-corrected ("difference") mass spectra. We calibrate the ACSM using 300 nm size-selected ammonium nitrate and ammonium sulfate aerosols generated from nebulized 0.005 M solutions using the Aerosol Generation System (Brechtel, AGS 2002). We determine the appropriate nitrate response factor (RF) and relative ionization efficiencies (RIEs) for ammonium and sulfate and use these factors to convert ion intensities to mass concentrations. We use the standard ion fragmentation table to allocate the ion fragments to different bulk species: organics, sulfate, nitrate, ammonium, or chloride.

We correct the organic aerosol (Org) trace for wall losses following the organic-to-sulfate ratio method described in Hildebrandt et al. 53 In this method, the ACSM Org concentration is multiplied by the mass concentration ratio of initial sulfate (measured by the SEMS) over the time-dependent sulfate (measured by the ACSM) to produce a wall-loss corrected Org concentration. This method accounts for particle wall losses and the partitioning of organic vapors to wall-deposited particles but does not account for the loss of vapors to the Teflon chamber walls. The method assumes

internal mixing of particles and that organic vapors partition to wall-deposited particles as if they were suspended.

We use the ACSM to calculate SOA mass yields for experiments 1-8 as follows:

SOA yield =
$$\frac{C_{\text{OA}}[\mu \text{ gm}^{-3}]}{\Delta \text{VOC}[\mu \text{ gm}^{-3}]}$$
(3)

where C_{OA} is the concentration of organic aerosol formed (corrected as described above) and ΔVOC is the amount of α -pinene reacted. Since the chamber is particle-free before every experiment, the initial amount of C_{OA} is zero, and the final amount of C_{OA} is the maximum concentration of OA formed. ΔVOC is the initial amount of VOC injected assuming complete consumption (section 2.2). We do not calculate SOA mass yields for OH experiments (9 and 10), as we cannot assume complete consumption of OH for these experiments.

We also use the ACSM data to calculate f_{44} , the fraction of total organic aerosol due to species at m/z 44 (mostly the fragment ion $\mathrm{CO_2}^+$), which is a proxy for the extent of oxidation of organic aerosol. Detailed ACSM analysis suggests that the nitrate (NO₃) measured is due to organic nitrates (see section S.3), and the fraction of nitrate is shown as f_{NO3} (i.e., NO₃/Org) in Table 1.

In the following discussion, we will refer to a "base case" experiment (exp 2 in Table 1) where the ratio of VOC:NO:Cl₂ was 1:1:1 with an initial injection of 15 ppb of each reactant, a moderate RH of 40% was maintained, and inorganic ammonium sulfate seed was injected.

3. RESULTS AND DISCUSSION

Experimental conditions and results are summarized in Table 1. We varied temperature, NO_x levels, VOC, and oxidant precursor levels (while keeping VOC: Cl_2 ratio at 1) and conducted two experiments (exp 9, 10) with OH radicals as the oxidant to compare SOA and HOM formation from Clversus OH-initiated chemistry.

3.1. Gas and Particle Phase Products. Figure 1 shows time series from a representative α -pinene+Cl+NO experiment with the highest initial precursor concentration and SOA formed (exp 5). The figure shows gas-phase time series based on I⁻ CIMS data, as well as organic aerosol concentration based on the ACSM Org signal. The traces shown are of select

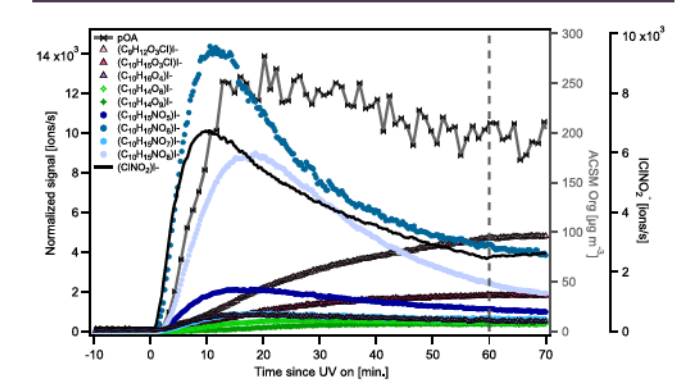


Figure 1. Gas phase time series based on I⁻ CIMS data for exp 5. The vertical dotted line indicates the time at which UV lights were turned off. The pOA signal is based on the wall-loss corrected ACSM Org signal. Traces shown are of select abundant species in the gas phase, and include chlorinated, nitrated, and highly oxygenated species.

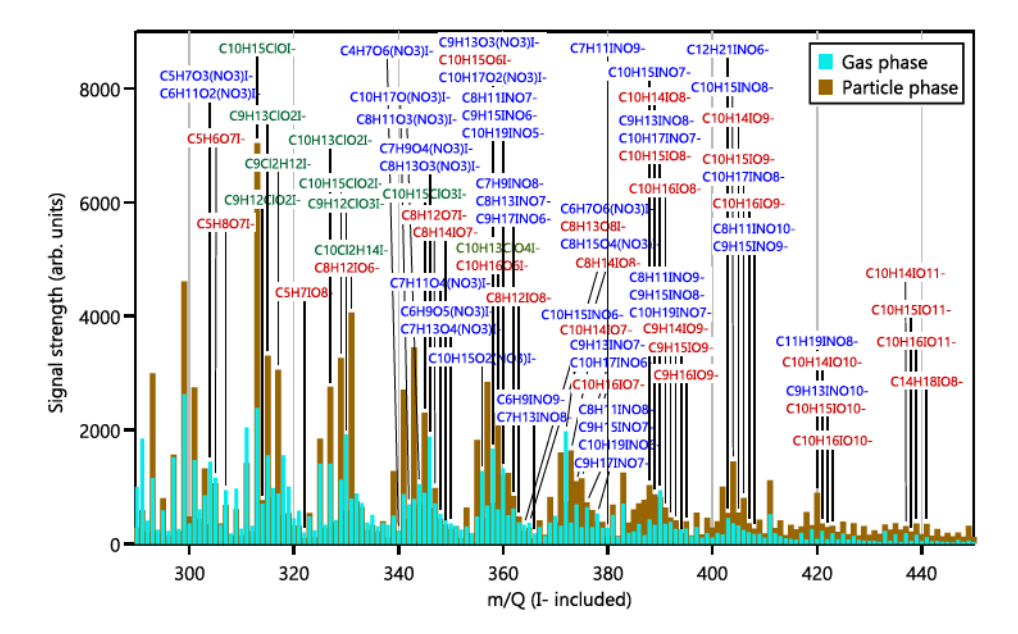


Figure 2. Average unit mass resolution mass spectrum for exp 5 based on FIGAERO-CIMS data, showing gas and particle phase composition from the same sampling period. Several classes of compounds including organic chlorides (green formulas), organic nitrates (blue formulas), and highly oxygenated organic molecules (red formulas) are observed in both phases. Labeling of compounds is based on high-resolution fitting of peaks in the CIMS spectra. m/z scale ends at 450 in spectrum, but more compounds are observed (at lower concentrations) up to m/z 639.

highly abundant monomeric (C_9 , C_{10}) compounds clustered with the reagent ion (I^-) that evolve from the α -pinene+Cl +NO reaction. Similar time series for exp 3 and 4, and a full list of compounds detected by the I^- CIMS are provided in the SI (Figure S2 and Table S1).

As α -pinene is oxidized by Cl, gas-phase products form almost immediately, and maximum SOA concentration is observed within ~20 min. This is due to the fast reaction rates for Cl-initiated oxidation of α -pinene, and high Cl concentrations in the chamber. Abundant monomeric reaction products include chlorinated products such as CoH12O3Cl and C₁₀H₁₅O₃Cl, plain organics such as C₁₀H₁₄O_{8,9} (see Figure S9 and S10 for HR-fits), C₁₀H₁₆O₄, and nitrated organics such as C10H15NO5-8. Most gas-phase products peak at different times and then decline. Gas-phase ClNO2 rises immediately upon illumination, reaches its peak at the 10 min mark, and then steadily declines until the lights are turned off due to photolysis. The concentration of organic aerosol (pOA) also decreases after reaching a maximum until lights are turned off, consistent with a role of photolysis in the decline. Several HOM appear within minutes of the start of photo-oxidation, consistent with these compounds being autoxidation products (as opposed to multigenerational or sequential oxidation products that appear later), as atmospheric autoxidation reactions have been found to occur on the time scale of a few seconds to minutes. 52,55-57

Hundreds of products are formed from the Cl-initiated oxidation of α -pinene, several of which are detected in both the gas and particle phases. Figure 2 shows an example mass spectrum of gas and particle-phase compounds from exp 5, shown as blue and brown bars, respectively. The mass spectrum is an average spectrum based on unit mass resolution data; however, peaks are labeled according to HR-identified compounds from the I⁻ ToF-CIMS based on the high-resolution peak fitting procedure outlined in section 2.2. We sampled gas-phase products and collected aerosol for 30 min

after the lights were turned off. The gas-phase mass spectrum is an average of those 30 min, while the particle-phase spectrum is based on the average desorption signals resulting from the collected particles over the same 30 min period. The full list of compounds detected by the I^- CIMS in the gas and particle phases is provided in the SI (see section S.10).

Several compound classes including chlorinated products, chlorinated and nonchlorinated HOM, nitrates, and some dimers are shown. Toward the lower m/z region, the gas-phase contribution is more prominent, while at higher m/z, the particle phase dominates. This is consistent with larger molecules having lower vapor pressures and therefore more readily partitioning to the particle phase. HOM are present in considerable amounts in both the gas and particle phases. The presence of chlorinated HOM is indicative that the Cl-addition pathway forms chlorinated RO₂ precursors that can undergo autoxidation. Several dimers are also observed in the CIMS mass spectra (not shown on the graph for scaling purposes) indicating the importance of oligomerization reactions in the α-pinene+Cl system. Examples of such dimers include $C_{16}H_{29}NO_8$, $C_{18}H_{28}O_{10-11}$, $C_{19}H_{28}O_{8-9}$, $C_{19}H_{30}O_{8-10}$, $C_{20}H_{30}O_{12-13}$, and $C_{20}H_{32}O_{9,11-13}$ (also see section S.10). The presence of NO_x in the chamber results in the formation of OH and O₃ which can oxidize α -pinene. However, modeling of exp 2 (base case experiment, see section S.7 for more modeling details) shows that the lifetimes of α -pinene (averaged over the first 8 min, when most of the α -pinene is consumed) with respect to oxidation by O3, OH, and Cl radicals are 7×10^4 , 600, and 100 s, respectively, indicating that Cl radicals are the dominant oxidant (see section S.7 in Supporting Information). While average Cl concentrations in this experiment set are higher than they are in usual atmospheric contexts, 27,58 we choose these higher concentrations specifically to bias the reaction toward the α -pinene +Cl pathway.

$$\begin{array}{c} \text{CI} \\ \text{HI}_{15} \text{CIO}_{3.5,7} \\ \text{CI} \\ \text{H-shift} \\ \text{CI} \\ \text{CI} \\ \text{H-shift} \\ \text{CI} \\ \text{CI}_{10} \\ \text{H}_{15} \\ \text{CIO}_{2.4,6} \\ \text{CI}_{10} \\ \text{H}_{17} \\ \text{CIO}_{6.8,10} \\ \text{CI} \\ \text{OOH} \\ \text{OOH} \\ \end{array}$$

Figure 3. Select oxidation pathways for the α -pinene + Cl reaction leading to autoxidation and formation of HOM. An initial peroxy radical can be formed via Cl-addition or H-abstraction after which autoxidation (addition of O_2) can occur. The termination products shown here are examples.

Data from the unit mass resolution spectrum of the ACSM can be used to explore particle composition, as described in section 2.3. For exp 5, the f_{44} value (proxy for extent of oxidation³⁶) is 0.11. This value is slightly lower than the base case values (0.15 for exp 2, and 0.13 for exp 6), consistent with less oxidized products partitioning to the particle phase under the higher organic aerosol concentrations in exp 5. The $f_{\rm NO3}$ value (NO₃/Org) was low for all experiments and did not always follow expected trends. For example, $f_{\rm NO3}$ was the same for the base case (exp 2) and low NO_x experiment (exp 3). These observations are indicative of overall low levels of organic nitrates in the particle phase, and interference from organic ions in the calculation of NO₃ from the ACSM.⁵⁹

3.1.1. Highly Oxygenated Organic Molecules (HOM). The reaction of α -pinene with Cl radicals can lead to HOM formation. We define HOM as non-nitrated molecules containing six or more oxygen atoms which are likely formed via auto-oxidation of peroxy radicals in the gas phase, consistent with the criteria suggested by Bianchi et al. We define nitrated HOM as nitrated molecules having at least eight oxygen atoms. We limit our HOM analysis to monomers (C_9-C_{10}) only, to eliminate the possibility of highly functionalized dimers (which may have been formed through a pathway other than autoxidation) being counted as HOM. Some HOM formation pathways are similar to HOM formation from reaction with OH; others would be considered negligible for oxidation with OH.

Figure 3 outlines a proposed mechanism for the formation of select chlorinated and nonchlorinated autoxidation products, including HOM, from the α -pinene + Cl reaction. The NO addition pathway is excluded from the proposed mechanism for simplicity. The bottom oxidation pathway follows an initial H-abstraction step, while the oxidation steps on the right follow initial Cl-addition. Cl can be lost after the initial Cl-addition step; ¹³ thus, our data cannot be used to quantify the fraction of reactions occurring via H-abstraction versus Cl-addition. Several of the proposed final products in the mechanism are shown in the gas-phase time series in Figure 1 ($C_{10}H_{15}ClO_3$, $C_{10}H_{14}O_{8,9}$) and are observed in the gas and particle phases in the FIGAERO—CIMS. We note here that

the FIGAERO-CIMS cannot distinguish between isomers, so it is possible that the compounds we have identified have a different structure and/or are formed from different pathways.

One potential difference in the reaction of α -pinene with Cl (compared to with OH) is the increased propensity for H-abstraction relative to addition 19 and the capability for Cl to abstract primary H to an appreciable extent. 63 When initial oxidation proceeds through H-abstraction, the potential will exist for fast unimolecular reactions due to the retention of the double bond, as illustrated in Figure 3. H-abstraction at primary sites will potentially lead to unique/novel reaction pathways, as H shifts from primary RO2 tend to occur at differ rates than from secondary or tertiary RO2. 64 Abstraction of primary H can also potentially lead to the formation of peroxy acyl radical or aldehyde groups, 65 which tend to undergo internal H shifts at faster rates than other functionalities. 64

Table 1 shows the fraction of HOM in the particle phase $(F_{\rm p})$ based on CIMS data for the experiment set. An $F_{\rm p}$ of 1 indicates that all HOM are in the particle phase; an $F_{\rm p}$ of 0.5 indicates that the HOM formed are distributed equally between the gas and particle phases. For this experiment set, up to 85% of HOM are in the particle phase, suggesting the importance of considering particle-phase concentrations when evaluating HOM. The partitioning of HOM to the particle phase is greatest for exp 5 and exp 7 which are the experiments with the highest organic aerosol loadings. In fact, overall there is a positive correlation between the fraction of HOM in the particle phase and the concentration of organic aerosol in the chamber. This suggests that the gas-particle distribution of HOM is impacted by equilibrium partitioning and that HOM do not irreversibly condense to particles.

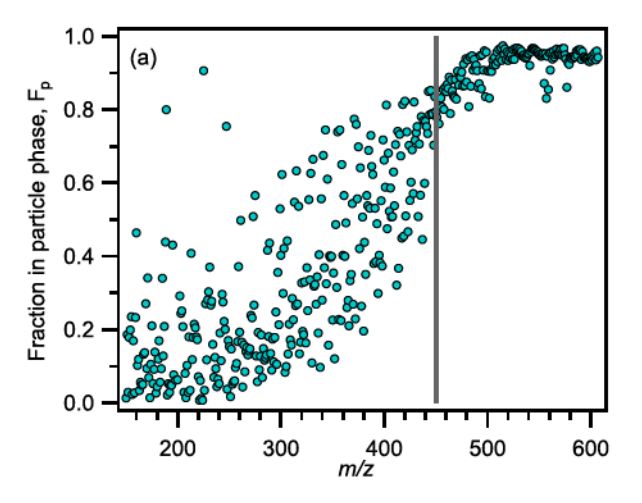
3.1.2. Particle Composition from ACSM Data. We utilize ACSM unit mass resolution data to further explore the differences in particle-phase composition for this experiment set. Under high NO_x conditions, we observe that OH-initiated oxidation (exp 10) results in a comparable fraction of NO_3 formed (6%) compared to Cl-initiated oxidation (exp 6, 7%). Comparing exp 1 (RH < 5%) and exp 2 (RH ~40%), f_{NO3} is 8% for the dry conditions and 3% for the "humid" conditions. The lower nitrate concentration under humid conditions could

indicate that hydrolysis is a possible sink of alkyl nitrates in this system. Previous studies on OH-initiated oxidation of α -pinene have shown that hydrolysis may be a dominant loss mechanism for α -pinene-derived organic nitrates in the aerosol phase. 60 Specifically, Takeuchi and Ng68 reported a hydrolysis lifetime for the α-pinene+OH system of less than 30 min, with the hydrolyzable fraction of organic nitrates ranging from 23-32%, indicating that hydrolysis may indeed be a dominant loss mechanism for particulate organic nitrates. Finally, comparing exp 7 (5 °C), exp 6 (25 °C), and exp 8 (40 °C), we see that $f_{\rm NO3}$ decreases as the temperature increases (8.3% to 7.2% to 6.5%). This could be due to organic nitrates having a higher average volatility than non-nitrated organics or possibly due to the variation of organonitrate production rates at different temperatures. Comparing exp 2 (base case) to exp 3 (low NO_x), although NO was not added to the chamber in exp 3, we observe from CIMS spectra that nitrated organics form in the gas phase, albeit at lower concentrations. This is likely due to NOx off-gassing from the Teflon chamber walls as previously observed in smog chambers⁶⁹ and may explain the comparable f_{NO3} values for exp 2 and 3.

In terms of the extent of oxidation of organic aerosol, a negative correlation between f_{44} and SOA concentration is seen for the Cl-initiated oxidation experiments on average (excluding the low and high temperature experiments 7 and 8). As the organic aerosol loading in the chamber increases, more volatile (and generally less oxidized) species partition into the particle-phase, lowering the extent of oxidation of the organic aerosol. Overall, the SOA formed from Cl-initiated reactions appears to be more highly oxidized than SOA formed in OH-initiated reactions. The f_{44} of SOA formed in exp 10 (OH+NO) is 0.07 versus 0.15 for exp 2 (Cl+NO); likewise, f_{44} of SOA formed in exp 9 (low NO, OH) is 0.08 versus 0.10 for exp 3 (low NOx, Cl). A higher OA oxidation state from Clinitiated reactions is consistent with faster chemistry resulting in the rapid formation of more oxidized species which have lower volatility and therefore have the potential to form SOA at higher mass yields. Based on these observations, we hypothesize that the RO₂ radical concentration in the chamber is not high enough where it begins to inhibit autoxidation.

3.2. SOA Partitioning. We study the volatility behavior of the SOA produced from Cl-initiated oxidation of α -pinene in two ways: (1) two-dimensional thermograms and (2) partitioning values (F_p), as described in section 2.2. We utilize the ToF-CIMS unit mass resolution data for both methods to allow for a direct comparison, as shown in Figure 4. The F_p in Figure 5 are based on high resolution peak identification. Two-dimensional thermograms are available for all experiments (except exp 6 due to unavailability of FIGAERO data), and trends are briefly discussed in the SI (section S.6).

3.2.1. Partitioning Based on FIGAERO-CIMS. Following the procedure described in section 2.2, we calculate partitioning values (F_p) using unit mass resolution data and plot these against m/z as seen in Figure 4a. The plots shown in Figure 4 are for UMR data based on exp 5 which had the highest organic aerosol loading. The fraction of each compound in the particle phase shows a positive dependence on molecular size (m/z) though there is significant scatter at the lower end of the mass spectrum (< m/z) 440. F_p values plateau near $F_p = 0.97$ (rather than 1.0) likely due to uncertainties caused by subtraction of the gas-phase background. Figure 4b shows a 2D-thermogram from the same experiment, which we generated based on the procedure



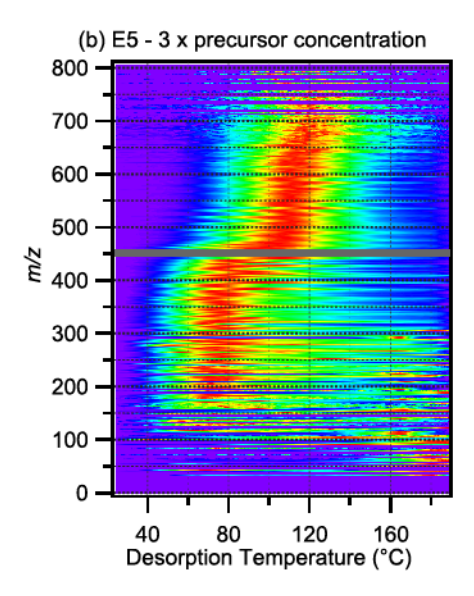


Figure 4. (a) Fraction of compounds in the particle phase (based on UMR data) vs m/z (b) Corresponding UMR 2-D thermogram showing "scatter" in lower m/z region. m/z value includes 127 from I⁻ reagent ion. Desorption behavior seen at $T_{\rm max} \sim 160~{}^{\circ}{\rm C}$ is attributed to desorption of inorganic (ammonium sulfate) seed.

described in section 2.2. The 2D thermogram shows desorption of species at a relatively wide range of temperatures at each m/z below 440, consistent with the range of scattered F_p values in Figure 4a. This is consistent with the presence of molecules of similar size but containing different functional groups, resulting in different vapor pressures. Beyond m/z 440, most molecules are either dimers or highly oxidized monomers which are predominantly present in the particle phase. The trend seen in Figure 4b is generally consistent with 2D thermograms for other experiments in this work (as seen in the SI, Figures S6 and S7). There are three distinct regions in the 2D-thermograms: the first region of m/z < 400 where T_{max} is relatively constant with m/z at around ~70 °C, the second region from \sim 450 < m/z < 500, characterized by an upward slope in T_{max} and the third (m/z > 500) with steady T_{max} values at ~110 °C. There is evidence of possible thermal fragementation for some of the experiments, characterized by unusually high T_{max} values at low m/z (<400).

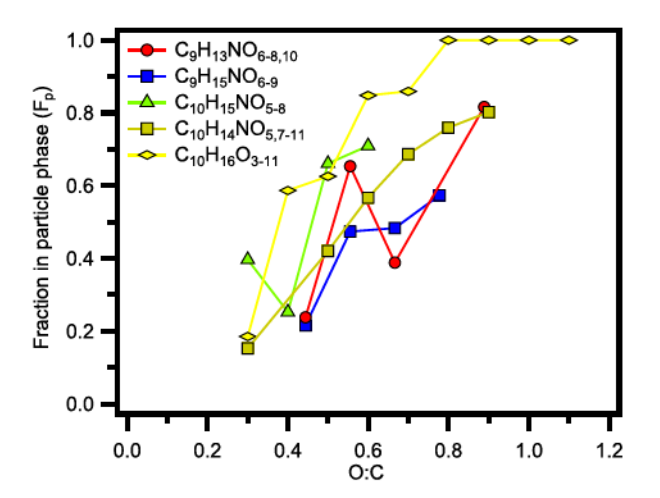


Figure 5. F_p vs effective O:C ratio for compounds with increasing number of oxygen atoms.

To further investigate the impact of functional groups on observed partitioning (F_p) , we select products of the α -pinene +Cl+NO reaction and plot their F_p against their effective oxygen to carbon ratio (O:C) as seen in Figure 5, which is based on high resolution CIMS data. We calculate effective O:C based on observed carbon and oxygen numbers with the subtraction of two oxygen atoms for each nitrogen atom. The compounds shown are select monomeric compounds that are found in "series" with an increasing number of O atoms.

The fraction of a compound in the particle phase generally increases with the number of O atoms in a compound, until it reaches a plateau at $F_p = 1$ which indicates that the compound is only found in the particle phase. It is evident from Figure 5 that even when composition is considered, an increase in O:C does not always translate to a linear increase in partitioning to the particle phase. This is expected given the lack of information about the functional group in which the O atom is present (for example, hydroxyl versus carbonyl). Although information on size (m/z) and O:C ratios can be reasonable predictors of volatility, knowledge on the structural identity of molecules is essential to fully determine the vapor pressure of species. The vapor pressures of functional group isomers (molecules of equivalent elemental formulas but different functional groups) can differ by 2-3 orders of magnitude. 71-74 Even positional isomers (isomers with the same functional groups on different positions in the carbon chain) can impact vapor pressures as they affect intra- and intermolecular hydrogen bonding.75

The temperature at which the maximum particle signal is observed $(T_{\rm max})$ has also been used in the literature to infer volatility of particle-phase species. $^{40,43-45,76,77}$ However, we find that $T_{\rm max}$ does not appear to be a reliable indicator of volatility. Although the fraction of a compound in the particle phase $(F_{\rm p})$ and its $T_{\rm max}$ should be positively correlated, most organic species desorb around a narrow $T_{\rm max}$ range (see Figure S4) making it difficult to see such a trend and to obtain volatility information from $T_{\rm max}$ values. For instance, the $T_{\rm max}$ values of $C_9H_{15}NO_8$ and $C_9H_{13}NO_{10}$ (Figure S4b) are similar at \sim 80 °C even though these compounds are expected to exhibit different desorption behaviors based on their different elemental formulas. We observe similar behavior (i.e., similar $T_{\rm max}$ values) for $C_{10}H_{14}O_7$ and $C_{10}H_{14}O_{11}$ from Figure S4b, and $C_{10}ClH_{15}O_2$ and $C_8H_{13}NO_6$ from Figure S4c. Further-

more, T_{max} is dependent on organic aerosol loading on the PTFE filter as reported by Huang et al. and Wang and Hildebrandt Ruiz^{17,78}, and as observed in this work (see Figure S5). Overall, FIGAERO-CIMS data can provide valuable insights into the partitioning behavior of species based on their size and elemental ratios. Calibrating the FIGAERO-CIMS with a variety of standards that cover a large span of molecular sizes and saturation concentrations can be beneficial for obtaining more reliable volatility information, but care must be taken to account for possible OA loading dependence, and when dealing with data sets which may contain positional or structural isomers. Using other analytical instrumentation that can distinguish between isomers (e.g., gas chromatographymass spectroscopy (GC-MS) or ion mobility spectrometry (IMS)) in tandem with FIGAERO-CIMS may also improve confidence in the volatility information obtained from FIGAERO data.

3.2.2. SOA Yields. We report secondary organic aerosol yields for experiments 1-8 and plot them against organic aerosol loading in Figure 6. We do not evaluate SOA yields

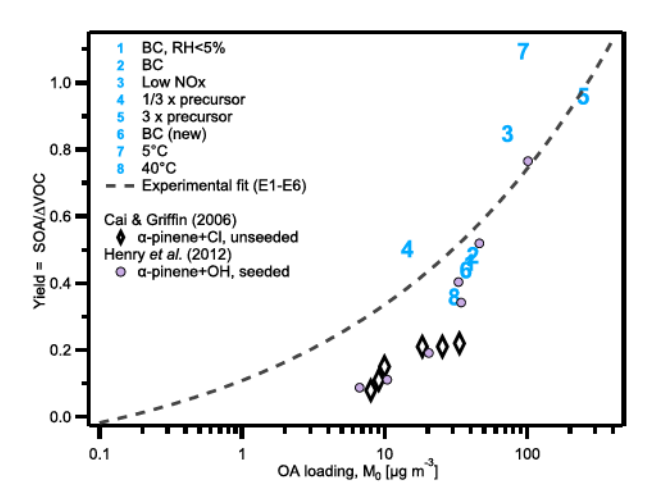


Figure 6. Plot of yield versus OA loading (log scale) based on ACSM data. Experiments from this work are labeled by experiment number as shown in Table 1. α -Pinene+Cl and α -pinene+OH chamber yield results from the literature are shown for comparison purposes. No NO_x species were added in the experiments by Cai and Griffin ¹³ and Henry et al. ⁷⁹ The dotted gray line is the yield curve based on a fit of the experiments (E1–E6) in this work.

from the OH experiments, as we were unable to measure the fraction of α -pinene consumed. SOA yields from this work are labeled by experiment number, and results from previous studies of the α -pinene+Cl¹³ and α -pinene+OH⁷⁹ systems are added for comparison. Overall, the SOA yields in this study are similar to those observed in previous work. Figure 6 shows that the fitted yield curve (based on exp 1–6) follows the expected behavior based on absorptive gas-particle partitioning theory. The lower yields for the α -pinene+Cl system discussed in work by Cai and Griffin compared to this work may be due to the absence of inorganic seed within their chamber, which can lead to higher wall losses, ^{81–83} and due to differences in the wall-loss correction method used.

By comparison of SOA yields from exp 4 and 5 (low vs high precursor concentration), it appears that SOA formation is moderately enhanced (relative to the yield curve) at lower precursor concentration. The organic aerosol formed in exp 4 is more oxidized than in exp 5 ($f_{44} = 0.14$ vs 0.11), and thus the higher SOA yields observed in exp 4 are consistent with more highly oxidized species having lower vapor pressure, resulting in increased partitioning to the particle phase.

Exp7 which was conducted at a low temperature of 5 °C lies highest above the yield curve, and exp 8 (high temperature) lies below the yield curve, consistent with the dependence of saturation vapor pressures on temperature, resulting in more OA formation at lower temperature. The "base case" experiments (1, 2, 6) lie very close to each other on the Yield—OA loading curve, indicating good repeatability within our environmental chamber. Overall, SOA yields from this experiment set show the importance of Cl chemistry in enhancing SOA formation in the atmosphere.

CONCLUSIONS

In this work, we find that Cl-initiated oxidation of α -pinene forms high yields of organic aerosol that is more highly oxygenated than aerosol formed from OH-initiated oxidation. High-resolution fitting of CIMS data shows that numerous HOM are present in the gas and particle phases at substantial levels, suggestive of the importance of auto-oxidation and the formation of HOM in the formation of SOA from α -pinene. We calculate the fraction of measured molecules in the particle phase (F_p) and find that F_p generally increases with molecular size and extent of oxidation; however, it is also clear that other factors impact volatility. Particle fractions of HOM appear to be influenced by equilibrium partitioning, suggesting that partitioning of HOM to the particle phase is not irreversible. Considering the rapid formation of oxygenated molecules and OA from Cl-initiated oxidation of α -pinene, Cl chemistry may be an important contributor to the formation of secondary pollutants especially in regions with high chlorine concentrations.

ASSOCIATED CONTENT

Supporting Information

The Supporting Information is available free of charge at https://pubs.acs.org/doi/10.1021/acsearthspace-chem.1c00150.

Schematic of the environmental chamber; time-series for exp 3 and 4; discussion of organic vs inorganic particulate NO_3 based on ACSM data; comparison of partitioning values to $T_{\rm max}$ and example 1-D thermograms for select species; discussion of $T_{\rm max}$ dependence on filter loading; two-dimensional thermograms; description of chamber modeling; example CIMS high resolution fits for HOM; time series for OH-initiated oxidation (exp 10); table of oxidation products identified from FIGAERO-CIMS data (PDF)

AUTHOR INFORMATION

Corresponding Author

Lea Hildebrandt Ruiz — McKetta Department of Chemical Engineering, The University of Texas at Austin, Austin, Texas 78712, United States; oorcid.org/0000-0001-8378-1882; Email: lhr@che.utexas.edu

Author

Catherine G. Masoud – McKetta Department of Chemical Engineering, The University of Texas at Austin, Austin, Texas 78712, United States Complete contact information is available at: https://pubs.acs.org/10.1021/acsearthspacechem.1c00150

Note

The authors declare no competing financial interest.

ACKNOWLEDGMENTS

This material is based upon work supported in part by the National Science Foundation under Grant No. 1653625 and the Welch Foundation under Grants No. F-1925-20170325 and F-1925-20200401. We thank all sponsors for their generous support. We thank Mrinali Modi for modeling the chamber experiments, and Dr. Leif Jahn for useful discussions about the HOM formation mechanism.

■ REFERENCES

- (1) Anderson, J. O.; Thundiyil, J. G.; Stolbach, A. Clearing the Air: A Review of the Effects of Particulate Matter Air Pollution on Human Health. *J. Med. Toxicol.* 2012, 8 (2), 166–175.
- (2) Burnett, R.; Chen, H.; Szyszkowicz, M.; Fann, N.; Hubbell, B.; Pope, C. A.; Apte, J. S.; Brauer, M.; Cohen, A.; Weichenthal, S.; Coggins, J.; Di, Q.; Brunekreef, B.; Frostad, J.; Lim, S. S.; Kan, H.; Walker, K. D.; Thurston, G. D.; Hayes, R. B.; Lim, C. C.; Turner, M. C.; Jerrett, M.; Krewski, D.; Gapstur, S. M.; Diver, W. R.; Ostro, B.; Goldberg, D.; Crouse, D. L.; Martin, R. V.; Peters, P.; Pinault, L.; Tjepkema, M.; van Donkelaar, A.; Villeneuve, P. J.; Miller, A. B.; Yin, P.; Zhou, M.; Wang, L.; Janssen, N. A. H.; Marra, M.; Atkinson, R. W.; Tsang, H.; Quoc Thach, T.; Cannon, J. B.; Allen, R. T.; Hart, J. E.; Laden, F.; Cesaroni, G.; Forastiere, F.; Weinmayr, G.; Jaensch, A.; Nagel, G.; Concin, H.; Spadaro, J. V. Global Estimates of Mortality Associated with Long-Term Exposure to Outdoor Fine Particulate Matter. *Proc. Natl. Acad. Sci. U. S. A.* 2018, 115 (38), 9592–9597.
- (3) Nel, A. Air Pollution—Related Illness: Effects of Particles. Science (Washington, DC, U. S.) 2005, 308 (5723), 804–806.
- (4) Pope, C. A.; Dockery, D. W. Health Effects of Fine Particulate Air Pollution: Lines That Connect. *J. Air Waste Manage. Assoc.* 2006, 56, 709–742.
- (5) Bellouin, N.; Quaas, J.; Gryspeerdt, E.; Kinne, S.; Stier, P.; Watson-Parris, D.; Boucher, O.; Carslaw, K. S.; Christensen, M.; Daniau, A. L.; Dufresne, J. L.; Feingold, G.; Fiedler, S.; Forster, P.; Gettelman, A.; Haywood, J. M.; Lohmann, U.; Malavelle, F.; Mauritsen, T.; McCoy, D. T.; Myhre, G.; Mülmenstädt, J.; Neubauer, D.; Possner, A.; Rugenstein, M.; Sato, Y.; Schulz, M.; Schwartz, S. E.; Sourdeval, O.; Storelvmo, T.; Toll, V.; Winker, D.; Stevens, B. Bounding Global Aerosol Radiative Forcing of Climate Change. Rev. Geophys. 2020, 1 DOI: 10.1029/2019RG000660.
- (6) Jimenez, J. L.; Canagaratna, M. R.; Donahue, N. M.; Prevot, a S. H.; Zhang, Q.; Kroll, J. H.; DeCarlo, P. F.; Allan, J. D.; Coe, H.; Ng, N. L.; Aiken, a C.; Docherty, K. S.; Ulbrich, I. M.; Grieshop, a P.; Robinson, a L.; Duplissy, J.; Smith, J. D.; Wilson, K. R.; Lanz, V. a; Hueglin, C.; Sun, Y. L.; Tian, J.; Laaksonen, A.; Raatikainen, T.; Rautiainen, J.; Vaattovaara, P.; Ehn, M.; Kulmala, M.; Tomlinson, J. M.; Collins, D. R.; Cubison, M. J.; Dunlea, E. J.; Huffman, J. a; Onasch, T. B.; Alfarra, M. R.; Williams, P. I.; Bower, K.; Kondo, Y.; Schneider, J.; Drewnick, F.; Borrmann, S.; Weimer, S.; Demerjian, K.; Salcedo, D.; Cottrell, L.; Griffin, R.; Takami, a; Miyoshi, T.; Hatakeyama, S.; Shimono, a; Sun, J. Y.; Zhang, Y. M.; Dzepina, K.; Kimmel, J. R.; Sueper, D.; Jayne, J. T.; Herndon, S. C.; Trimborn, a M.; Williams, L. R.; Wood, E. C.; Middlebrook, a M.; Kolb, C. E.; Baltensperger, U.; Worsnop, D. R. Evolution of Organic Aerosols in the Atmosphere. Science 2009, 326 (5959), 1525–1529.
- (7) Zhang, H.; Yee, L. D.; Lee, B. H.; Curtis, M. P.; Worton, D. R.; Isaacman-VanWertz, G.; Offenberg, J. H.; Lewandowski, M.; Kleindienst, T. E.; Beaver, M. R.; Holder, A. L.; Lonneman, W. A.; Docherty, K. S.; Jaoui, M.; Pye, H. O. T.; Hu, W.; Day, D. A.; Campuzano-Jost, P.; Jimenez, J. L.; Guo, H.; Weber, R. J.; de Gouw, J.; Koss, A. R.; Edgerton, E. S.; Brune, W.; Mohr, C.; Lopez-Hilfiker,

- F. D.; Lutz, A.; Kreisberg, N. M.; Spielman, S. R.; Hering, S. V.; Wilson, K. R.; Thornton, J. A.; Goldstein, A. H. Monoterpenes Are the Largest Source of Summertime Organic Aerosol in the Southeastern United States. *Proc. Natl. Acad. Sci. U. S. A.* 2018, 115 (9), 2038–2043.
- (8) Guenther, A. B.; Jiang, X.; Heald, C. L.; Sakulyanontvittaya, T.; Duhl, T.; Emmons, L. K.; Wang, X. The Model of Emissions of Gases and Aerosols from Nature Version 2.1 (MEGAN2.1): An Extended and Updated Framework for Modeling Biogenic Emissions., 5, 1503—1560. Geosci. Model Dev. 2012, 5, 1471—1492.
- (9) Yanez-Serrano, A. M.; Nolscher, A. C.; Bourtsoukidis, E.; Gomes Alves, E.; Ganzeveld, L.; Bonn, B.; Wolff, S.; Sa, M.; Yamasoe, M.; Williams, J.; Andreae, M. O.; Kesselmeier, J. Monoterpene Chemical Speciation in a Tropical Rainforest: Variation with Season, Height, and Time of Day at the Amazon Tall Tower Observatory (ATTO). Atmos. Chem. Phys. 2018, 18, 3403–3418.
- (10) Faxon, C. B.; Dhulipala, S. V.; Allen, D. T.; Hildebrandt Ruiz, L. Heterogeneous Production of Cl₂ from Particulate Chloride: Effects of Composition and Relative Humidity. *AIChE J.* 2018, 64 (8), 3151–3158.
- (11) Faxon, C.; Bean, J.; Hildebrandt Ruiz, L. Inland Concentrations of Cl2 and ClNO2 in Southeast Texas Suggest Chlorine Chemistry Significantly Contributes to Atmospheric Reactivity. *Atmosphere* 2015, 6, 1487–1506.
- (12) Thornton, J. a; Kercher, J. P.; Riedel, T. P.; Wagner, N. L.; Cozic, J.; Holloway, J. S.; Dubé, W. P.; Wolfe, G. M.; Quinn, P. K.; Middlebrook, A. M.; Alexander, B.; Brown, S. S. A Large Atomic Chlorine Source Inferred from Mid-Continental Reactive Nitrogen Chemistry. *Nature* 2010, 464 (7286), 271–274.
- (13) Cai, X.; Griffin, R. J. Secondary Aerosol Formation from the Oxidation of Biogenic Hydrocarbons by Chlorine Atoms. *J. Geophys. Res.* 2006, 111 (D14), D14206.
- (14) Wang, D.; Hildebrandt Ruiz, L. Secondary Organic Aerosol from Chlorine-Initiated Oxidation of Isoprene. *Atmos. Chem. Phys.* 2017, 17, 13491–13508.
- (15) Dhulipala, S. V.; Hildebrandt Ruiz, L. Oxidized Organic Compounds Formed from Chlorine-Initiated Oxidation of Toluene. *Atmos. Environ.* 2019, 199, 265–273.
- (16) Cai, X.; Ziemba, L. D.; Griffin, R. J. Secondary Aerosol Formation from the Oxidation of Toluene by Chlorine Atoms. *Atmos. Environ.* 2008, 42 (32), 7348–7359.
- (17) Wang, D. S.; Hildebrandt Ruiz, L. Chlorine-Initiated Oxidation of Alkanes under High-NO Conditions: Insights into Secondary Organic Aerosol Composition and Volatility Using a FIGAERO-CIMS. Atmos. Chem. Phys. 2018, 18 (21), 15535–15553.
- (18) Jahn, L. G.; Wang, D. S.; Dhulipala; Surya Venkatesh Hildebrandt Ruiz, L. Gas-Phase Chlorine Radical Oxidation of Alkanes: Effects of Structural Branching, NOx, and Relative Humidity Observed during Environmental Chamber Experiments. *J. Phys. Chem. A* 2021, 1 DOI: 10.1021/acs.jpca.1c03516.
- (19) Finlayson-Pitts, B. J.; Keoshian, C. J.; Buehler, B.; Ezell, A. A. Kinetics of Reaction of Chlorine Atoms with Some Biogenic Organics. *Int. J. Chem. Kinet.* 1999, 31 (7), 491–499.
- (20) Timerghazin, Q. K.; Ariya, P. A. Kinetics of the Gas-Phase Reaction of Atomic Chlorine with Selected Monoterpenes. *Phys. Chem. Chem. Phys.* 2001, 3 (18), 3981–3986.
- (21) Gill, K. J.; Hites, R. A. Rate Constants for the Gas-Phase Reactions of the Hydroxyl Radical with Isoprene, α and β -Pinene, and Limonene as a Function of Temperature. *J. Phys. Chem. A* 2002, 106 (11), 2538–2544.
- (22) Walavalkar, M.; Sharma, A.; Alwe, H. D.; Pushpa, K. K.; Dhanya, S.; Naik, P. D.; Bajaj, P. N. Cl Atom Initiated Oxidation of 1-Alkenes under Atmospheric Conditions. *Atmos. Environ.* 2013, 67, 93–100
- (23) Orlando, J. J.; Tyndall, G. S.; Bilde, M.; Ferronato, C.; Wallington, T. J.; Vereecken, L.; Peeters, J. Laboratory and Theoretical Study of the Oxy Radicals in the OH- and Cl-Initiated Oxidation of Ethene. J. Phys. Chem. A 1998, 102 (42), 8116–8123.

- (24) Atkinson, R.; Baulch, D. L.; Cox, R. A.; Crowley, J. N.; Hampson, R. F.; Hynes, R. G.; Jenkin, M. E.; Rossi, M. J.; Troe, J. Evaluated Kinetic and Photochemical Data for Atmospheric Chemistry: Volume II Gas Phase Reactions of Organic Species. *Atmos. Chem. Phys.* 2006, 6, 3625–4055.
- (25) Ofner, J.; Balzer, N.; Buxmann, J.; Grothe, H.; Schmitt-Kopplin, P.; Platt, U.; Zetzsch, C. Halogenation Processes of Secondary Organic Aerosol and Implications on Halogen Release Mechanisms. *Atmos. Chem. Phys.* 2012, 12 (13), 5787–5806.
- (26) Ofner, J.; Kamilli, K. A.; Held, A.; Lendl, B.; Zetzsch, C. Halogen-Induced Organic Aerosol (XOA): A Study on Ultra-Fine Particle Formation and Time-Resolved Chemical Characterization. *Faraday Discuss.* 2013, 165, 135.
- (27) Wang, Y.; Riva, M.; Xie, H.; Heikkinen, L.; Schallhart, S.; Zha, Q.; Yan, C.; He, X. C.; Peräkylä, O.; Ehn, M. Formation of Highly Oxygenated Organic Molecules from Chlorine-Atom-Initiated Oxidation of Alpha-Pinene. *Atmos. Chem. Phys.* 2020, 20 (8), 5145–5155.
- (28) Schervish, M.; Donahue, N. M. Peroxy Radical Chemistry and the Volatility Basis Set. Atmos. Chem. Phys. 2020, 20, 1183-1199.
- (29) Stolzenburg, D.; Fischer, L.; Vogel, A. L.; Heinritzi, M.; Schervish, M.; Simon, M.; Wagner, A. C.; Dada, L.; Ahonen, L. R.; Amorim, A.; Baccarini, A.; Bauer, P. S.; Baumgartner, B.; Bergen, A.; Bianchi, F.; Breitenlechner, M.; Brilke, S.; Mazon, S. B.; Chen, D.; Dias, A.; Draper, D. C.; Duplissy, J.; Haddad, I. El; Finkenzeller, H.; Frege, C.; Fuchs, C.; Garmash, O.; Gordon, H.; He, X.; Helm, J.; Hofbauer, V.; Hoyle, C. R.; Kim, C.; Kirkby, J.; Kontkanen, J.; Kürten, A.; Lampilahti, J.; Lawler, M.; Lehtipalo, K.; Leiminger, M.; Mai, H.; Mathot, S.; Mentler, B.; Molteni, U.; Nie, W.; Nieminen, T.; Nowak, J. B.; Ojdanic, A.; Onnela, A.; Passananti, M.; Petäjä, T.; Quéléver, L. L. J.; Rissanen, M. P.; Sarnela, N.; Schallhart, S.; Tauber, C.; Tomé, A.; Wagner, R.; Wang, M.; Weitz, L.; Wimmer, D.; Xiao, M.; Yan, C.; Ye, P.; Zha, Q.; Baltensperger, U.; Curtius, J.; Dommen, J.; Flagan, R. C.; Kulmala, M.; Smith, J. N.; Worsnop, D. R.; Hansel, A.; Donahue, N. M.; Winkler, P. M. Rapid Growth of Organic Aerosol Nanoparticles over a Wide Tropospheric Temperature Range. Proc. Natl. Acad. Sci. U. S. A. 2018, 115 (37), 9122-9127.
- (30) Tröstl, J.; Chuang, W. K.; Gordon, H.; Heinritzi, M.; Yan, C.; Molteni, U.; Ahlm, L.; Frege, C.; Bianchi, F.; Wagner, R.; Simon, M.; Lehtipalo, K.; Williamson, C.; Craven, J. S.; Duplissy, J.; Adamov, A.; Almeida, J.; Bernhammer, A. K.; Breitenlechner, M.; Brilke, S.; Dias, A.; Ehrhart, S.; Flagan, R. C.; Franchin, A.; Fuchs, C.; Guida, R.; Gysel, M.; Hansel, A.; Hoyle, C. R.; Jokinen, T.; Junninen, H.; Kangasluoma, J.; Keskinen, H.; Kim, J.; Krapf, M.; Kürten, A.; Laaksonen, A.; Lawler, M.; Leiminger, M.; Mathot, S.; Möhler, O.; Nieminen, T.; Onnela, A.; Petäjä, T.; Piel, F. M.; Miettinen, P.; Rissanen, M. P.; Rondo, L.; Sarnela, N.; Schobesberger, S.; Sengupta, K.; Sipilä, M.; Smith, J. N.; Steiner, G.; Tomè, A.; Virtanen, A.; Wagner, A. C.; Weingartner, E.; Wimmer, D.; Winkler, P. M.; Ye, P.; Carslaw, K. S.; Curtius, J.; Dommen, J.; Kirkby, J.; Kulmala, M.; Riipinen, I.; Worsnop, D. R.; Donahue, N. M.; Baltensperger, U. The Role of Low-Volatility Organic Compounds in Initial Particle Growth in the Atmosphere. Nature 2016, 533 (7604), 527-531.
- (31) Simon, M.; Dada, L.; Heinritzi, M.; Scholz, W.; Stolzenburg, D.; Fischer, L.; Wagner, A. C.; Kurten, A.; Rorup, B.; He, X.-C.; Almeida, J.; Baalbaki, R.; Baccarini, A.; Bauer, P. S.; Beck, L.; Bergen, A.; Bianchi, F.; Brakling, S.; Brilke, S.; Caudillo, L.; Chen, D.; Chu, B.; Dias, A.; Draper, D. C.; Duplissy, J.; El-Haddad, I.; Finkenzeller, H.; Frege, C.; Gonzalez-Carracedo, L.; Gordon, H.; Granzin, M.; Hakala, J.; Hofbauer, V.; Hoyle, C. R.; Kim, C.; Kong, W.; Lamkaddam, H.; Lee, C. P.; Lehtipalo, K.; Leiminger, M.; Mai, H.; Manninen, H. E.; Marie, G.; Marten, R.; Mentler, B.; Molteni, U.; Nichman, L.; Nie, W.; Ojdanic, A.; Onnela, A.; Partoll, E.; Petaja, T.; Pfeifer, J.; Philippov, M.; Quelever, L. L. J.; Ranjithkumar, A.; Rissanen, M. P.; Schallhart, S.; Schobesberger, S.; Schuchmann, S.; Shen, J.; Sipila, M.; Steiner, G.; Stozhkov, Y.; Tauber, C.; Tham, Y. J.; Tome, A. R.; Vazquez-Pufleau, M.; Vogel, A. L.; Wagner, R.; Wang, M.; Wang, D. S.; Wang, Y.; Weber, S. K.; Wu, Y.; Xiao, M.; Yan, C.; Ye, P.; Ye, Q.; Zauner-Wieczorek, M.; Zhou, X.; Baltensperger, U.; Dommen, J.;

- Flagan, R. C.; Hansel, A.; Kulmala, M.; Volkamer, R.; Winkler, P. M.; Worsnop, D. R.; Donahue, N. M.; Kirkby, J.; Curtius, J. Molecular Understanding of New-Particle Formation from α -Pinene between -50 and +25 °C. Atmos. Chem. Phys. 2020, 20 (15), 9183-9207.
- (32) Pospisilova, V.; Lopez-Hilfiker, F. D.; Bell, D. M.; Haddad, I. El; Mohr, C.; Huang, W.; Heikkinen, L.; Xiao, M.; Dommen, J.; Prevot, A. S. H.; Baltensperger, U.; Slowik, J. G. On the Fate of Oxygenated Organic Molecules in Atmospheric Aerosol Particles. *Sci. Adv.* 2020, 6 (11), eaax8922.
- (33) Ehn, M.; Thornton, J. A.; Kleist, E.; Sipilä, M.; Junninen, H.; Pullinen, I.; Springer, M.; Rubach, F.; Tillmann, R.; Lee, B.; Lopez-Hilfiker, F.; Andres, S.; Acir, I.-H.; Rissanen, M.; Jokinen, T.; Schobesberger, S.; Kangasluoma, J.; Kontkanen, J.; Nieminen, T.; Kurtén, T.; Nielsen, L. B.; Jørgensen, S.; Kjaergaard, H. G.; Canagaratna, M.; Maso, M. D.; Berndt, T.; Petäjä, T.; Wahner, A.; Kerminen, V.-M.; Kulmala, M.; Worsnop, D. R.; Wildt, J.; Mentel, T. F. A Large Source of Low-Volatility Secondary Organic Aerosol. Nature 2014, 506 (7489), 476–479.
- (34) Bianchi, F.; Kurtén, T.; Riva, M.; Mohr, C.; Rissanen, M. P.; Roldin, P.; Berndt, T.; Crounse, J. D.; Wennberg, P. O.; Mentel, T. F.; Wildt, J.; Junninen, H.; Jokinen, T.; Kulmala, M.; Worsnop, D. R.; Thornton, J. A.; Donahue, N.; Kjaergaard, H. G.; Ehn, M. Highly Oxygenated Organic Molecules (HOM) from Gas-Phase Autoxidation Involving Peroxy Radicals: A Key Contributor to Atmospheric Aerosol. *Chem. Rev.* 2019, 119 (6), 3472–3509.
- (35) Roldin, P.; Ehn, M.; Kurtén, T.; Olenius, T.; Rissanen, M. P.; Sarnela, N.; Elm, J.; Rantala, P.; Hao, L.; Hyttinen, N.; Heikkinen, L.; Worsnop, D. R.; Pichelstorfer, L.; Xavier, C.; Clusius, P.; Öström, E.; Petäjä, T.; Kulmala, M.; Vehkamäki, H.; Virtanen, A.; Riipinen, I.; Boy, M. The Role of Highly Oxygenated Organic Molecules in the Boreal Aerosol-Cloud-Climate System. *Nat. Commun.* 2019, 10 (1), 1–15.
- (36) Ng, N. L.; Herndon, S. C.; Trimborn, a.; Canagaratna, M. R.; Croteau, P. L.; Onasch, T. B.; Sueper, D.; Worsnop, D. R.; Zhang, Q.; Sun, Y. L.; Jayne, J. T. An Aerosol Chemical Speciation Monitor (ACSM) for Routine Monitoring of the Composition and Mass Concentrations of Ambient Aerosol. *Aerosol Sci. Technol.* 2011, 45 (7), 780–794.
- (37) Aljawhary, D.; Lee, A. K. Y.; Abbatt, J. P. D. High-Resolution Chemical Ionization Mass Spectrometry (ToF-CIMS): Application to Study SOA Composition and Processing. *Atmos. Meas. Tech.* 2013, 6 (11), 3211–3224.
- (38) Bertram, T. H.; Kimmel, J. R.; Crisp, T. a.; Ryder, O. S.; Yatavelli, R. L. N.; Thornton, J. a.; Cubison, M. J.; Gonin, M.; Worsnop, D. R. A Field-Deployable, Chemical Ionization Time-of-Flight Mass Spectrometer. *Atmos. Meas. Tech.* 2011, 4 (7), 1471–1479.
- (39) Lee, B. H.; Lopez-Hilfiker, F. D.; Mohr, C.; Kurtén, T.; Worsnop, D. R.; Thornton, J. a. An Iodide-Adduct High-Resolution Time-of-Flight Chemical-Ionization Mass Spectrometer: Application to Atmospheric Inorganic and Organic Compounds. *Environ. Sci. Technol.* 2014, 48 (11), 6309–6317.
- (40) Lopez-Hilfiker, F. D.; Mohr, C.; Ehn, M.; Rubach, F.; Kleist, E.; Wildt, J.; Mentel, T. F.; Lutz, A.; Hallquist, M.; Worsnop, D.; Thornton, J. A. A Novel Method for Online Analysis of Gas and Particle Composition: Description and Evaluation of a Filter Inlet for Gases and AEROsols (FIGAERO). Atmos. Meas. Tech. 2014, 7, 983—1001.
- (41) Lopez-Hilfiker, F. D.; Iyer, S.; Mohr, C.; Lee, B. H.; Kurten, T.; Thornton, J. A. Constraining the Sensitivity of Iodide Adduct Chemical Ionization Mass Spectrometry to Multifunctional Organic Molecules Using the Collision Limit and Thermodynamic Stability of Iodide Ion Adducts. *Atmos. Meas. Tech.* 2016, 9, 1505–1512.
- (42) Brophy, P.; Farmer, D. A Switchable Reagent Ion High Resolution Time-of-Flight Chemical Ionization Mass Spectrometer for Real-Time Measurement of Gas Phase Oxidized Species: Characterization from the 2013 Southern Oxidant and Aerosol Study. Atmos. Meas. Tech. 2015, 8, 2945.

- (43) Stark, H.; Yatavelli, R. L. N.; Thompson, S. L.; Kang, H.; Krechmer, J. E.; Kimmel, J. R.; Palm, B. B.; Hu, W.; Hayes, P. L.; Day, D. A.; Campuzano-Jost, P.; Canagaratna, M. R.; Jayne, J. T.; Worsnop, D. R.; Jimenez, J. L. Impact of Thermal Decomposition on Thermal Desorption Instruments: Advantage of Thermogram Analysis for Quantifying Volatility Distributions of Organic Species. *Environ. Sci. Technol.* 2017, 51 (15), 8491–8500.
- (44) Schobesberger, S.; Ambro, E. L.; Lopez-Hilfiker, F. D.; Mohr, C.; Thornton, J. A. A Model Framework to Retrieve Thermodynamic and Kinetic Properties of Organic Aerosol from Composition-Resolved Thermal Desorption Measurements. *Atmos. Chem. Phys.* 2018, 18 (20), 14757.
- (45) Lopez-Hilfiker, F. D.; Mohr, C.; Ehn, M.; Rubach, F.; Kleist, E.; Wildt, J.; Mentel, T. F.; Carrasquillo, A. J.; Daumit, K. E.; Hunter, J. F.; Kroll, J. H.; Worsnop, D. R.; Thornton, J. A. Phase Partitioning and Volatility of Secondary Organic Aerosol Components Formed from α-Pinene Ozonolysis and OH Oxidation: The Importance of Accretion Products and Other Low Volatility Compounds. *Atmos. Chem. Phys.* 2015, 15 (14), 7765–7776.
- (46) Kristensen, K.; Cui, T.; Zhang, H.; Gold, A.; Glasius, M.; Surratt, J. D. Dimers in α -Pinene Secondary Organic Aerosol: Effect of Hydroxyl Radical, Ozone, Relative Humidity and Aerosol Acidity. *Atmos. Chem. Phys.* 2014, 14 (8), 4201–4218.
- (47) Capouet, M.; Peeters, J.; Nozière, B.; Müller, J.-F. Alpha-Pinene Oxidation by OH: Simulations of Laboratory Experiments. *Atmos. Chem. Phys.* 2004, 4 (9/10), 2285–2311.
- (48) Molteni, U.; Simon, M.; Heinritzi, M.; Hoyle, C. R.; Bernhammer, A.-K.; Bianchi, F.; Breitenlechner, M.; Brilke, S.; Dias, A. A.; Duplissy, J.; Frege, C.; Gordon, H.; Heyn, C.; Jokinen, T.; Kü, A.; Lehtipalo, K.; Makhmutov, V.; Petä, T.; Pieber, S. M.; Praplan, A. P.; Schobesberger, S.; Steiner, G.; Stozhkov, Y.; António, A.; Tomé, T.; Trö Stl, J.; Wagner, A. C.; Wagner, R.; Williamson, C.; Yan, C.; Baltensperger, U.; Curtius, J.; Donahue, N. M.; Hansel, A.; Kirkby, J.; Kulmala, M.; Worsnop, D. R.; Dommen, J. Formation of Highly Oxygenated Organic Molecules from α-Pinene Ozonolysis: Chemical Characteristics, Mechanism, and Kinetic Model Development. ACS Earth Sp. Chem. 2019, 3, 873–883.
- (49) Kirkby, J.; Duplissy, J.; Sengupta, K.; Frege, C.; Gordon, H.; Williamson, C.; Heinritzi, M.; Simon, M.; Yan, C.; Almeida, J.; Tröstl, J.; Nieminen, T.; Ortega, I. K.; Wagner, R.; Adamov, A.; Amorim, A.; Bernhammer, A.-K.; Bianchi, F.; Breitenlechner, M.; Brilke, S.; Chen, X.; Craven, J.; Dias, A.; Ehrhart, S.; Flagan, R. C.; Franchin, A.; Fuchs, C.; Guida, R.; Hakala, J.; Hoyle, C. R.; Jokinen, T.; Junninen, H.; Kangasluoma, J.; Kim, J.; Krapf, M.; Kürten, A.; Laaksonen, A.; Lehtipalo, K.; Makhmutov, V.; Mathot, S.; Molteni, U.; Onnela, A.; Peräkylä, O.; Piel, F.; Petäjä, T.; Praplan, A. P.; Pringle, K.; Rap, A.; Richards, N. A. D.; Riipinen, I.; Rissanen, M. P.; Rondo, L.; Sarnela, N.; Schobesberger, S.; Scott, C. E.; Seinfeld, J. H.; Sipilä, M.; Steiner, G.; Stozhkov, Y.; Stratmann, F.; Tomé, A.; Virtanen, A.; Vogel, A. L.; Wagner, A. C.; Wagner, P. E.; Weingartner, E.; Wimmer, D.; Winkler, P. M.; Ye, P.; Zhang, X.; Hansel, A.; Dommen, J.; Donahue, N. M.; Worsnop, D. R.; Baltensperger, U.; Kulmala, M.; Carslaw, K. S.; Curtius, J. Ion-Induced Nucleation of Pure Biogenic Particles. Nature 2016, 533 (7604), 521-526.
- (50) Park, J.-H.; Babar, Z. B.; Baek, S. J.; Kim, H. S.; Lim, H.-J. Effects of NOx on the Molecular Composition of Secondary Organic Aerosol Formed by the Ozonolysis and Photooxidation of A-Pinene. *Atmos. Environ.* 2017, 166 (x), 263–275.
- (51) Jackson, S. R.; Harrison, J. C.; Ham, J. E.; Wells, J. R. A Chamber Study of Alkyl Nitrate Production Formed by Terpene Ozonolysis in the Presence of NO and Alkanes. *Atmos. Environ.* 2017, 171 (2), 143–148.
- (52) Rissanen, M. P.; Kurten, T.; Sipila, M.; Thornton, J. A.; Kausiala, O.; Garmash, O.; Kjaergaard, H. G.; Petaja, T.; Worsnop, D. R.; Ehn, M.; Kulmala, M. Effects of Chemical Complexity on the Autoxidation Mechanisms of Endocyclic Alkene Ozonolysis Products: From Methylcyclohexenes toward Understanding α -Pinene. *J. Phys. Chem. A* 2015, *119* (19), 4633–4650.

- (53) Hildebrandt, L.; Donahue, N. M.; Pandis, S. N. High Formation of Secondary Organic Aerosol from the Photo-Oxidation of Toluene. *Atmos. Chem. Phys.* 2009, *9*, 2973–2986.
- (54) Ng, N. L.; Canagaratna, M. R.; Zhang, Q.; Jimenez, J. L.; Tian, J.; Ulbrich, I. M.; Kroll, J. H.; Docherty, K. S.; Chhabra, P. S.; Bahreini, R.; Murphy, S. M.; Seinfeld, J. H.; Hildebrandt, L.; Donahue, N. M.; DeCarlo, P. F.; Lanz, V. A.; Prevot, A. S. H.; Dinar, E.; Rudich, Y.; Worsnop, D. R. Organic Aerosol Components Observed in Northern Hemispheric Datasets from Aerosol Mass Spectrometry. *Atmos. Chem. Phys.* 2010, 10, 4625–4641.
- (55) Berndt, T.; Richters, S.; Kaethner, R.; Voigtländer, J.; Stratmann, F.; Sipilä, M.; Kulmala, M.; Herrmann, H. Gas-Phase Ozonolysis of Cycloalkenes: Formation of Highly Oxidized RO2 Radicals and Their Reactions with NO, NO2, SO2, and Other RO2 Radicals. J. Phys. Chem. A 2015, 119 (41), 10336–10348.
- (56) Jokinen, T.; Sipilä, M.; Richters, S.; Kerminen, V. M.; Paasonen, P.; Stratmann, F.; Worsnop, D.; Kulmala, M.; Ehn, M.; Herrmann, H.; Berndt, T. Rapid Autoxidation Forms Highly Oxidized RO2 Radicals in the Atmosphere. *Angew. Chem., Int. Ed.* 2014, 53 (52), 14596–14600.
- (57) Rissanen, M. P.; Kurtén, T.; Sipilä, M.; Thornton, J. A.; Kangasluoma, J.; Sarnela, N.; Junninen, H.; Jørgensen, S.; Schallhart, S.; Kajos, M. K.; Taipale, R.; Springer, M.; Mentel, T. F.; Ruuskanen, T.; Petäjä, T.; Worsnop, D. R.; Kjaergaard, H. G.; Ehn, M. The Formation of Highly Oxidized Multifunctional Products in the Ozonolysis of Cyclohexene. *J. Am. Chem. Soc.* 2014, 136 (44), 15596–15606.
- (58) Tham, Y. J.; Wang, Z.; Li, Q.; Yun, H.; Wang, W.; Wang, X.; Xue, L.; Lu, K.; Ma, N.; Bohn, B.; Li, X.; Kecorius, S.; Größ, J.; Shao, M.; Wiedensohler, A.; Zhang, Y.; Wang, T. Significant Concentrations of Nitryl Chloride Sustained in the Morning: Investigations of the Causes and Impacts on Ozone Production in a Polluted Region of Northern China. Atmos. Chem. Phys. 2016, 16, 14959–14977.
- (59) Farmer, D. K.; Matsunaga, A.; Docherty, K. S.; Surratt, J. D.; Seinfeld, J. H.; Ziemann, P. J.; Jimenez, J. L. Response of an Aerosol Mass Spectrometer to Organonitrates and Organosulfates and Implications for Atmospheric Chemistry. *Proc. Natl. Acad. Sci. U. S. A.* 2010, 107 (15), 6670–6675.
- (60) Bianchi, F.; Kurtén, T.; Riva, M.; Mohr, C.; Rissanen, M. P.; Roldin, P.; Berndt, T.; Crounse, J. D.; Wennberg, P. O.; Mentel, T. F.; Wildt, J.; Junninen, H.; Jokinen, T.; Kulmala, M.; Worsnop, D. R.; Thornton, J. A.; Donahue, N.; Kjaergaard, H. G.; Ehn, M. Highly Oxygenated Molecules (HOM) from Gas-Phase Autoxidation Involving Organic Peroxy Radicals: A Key Contributor to Atmospheric Aerosol. *Chem. Rev.* 2019, 119 (6), 3472.
- (61) Møller, K. H.; Otkjær, R. V.; Chen, J.; Kjaergaard, H. G. Double Bonds Are Key to Fast Unimolecular Reactivity in First-Generation Monoterpene Hydroxy Peroxy Radicals. *J. Phys. Chem. A* 2020, 124 (14), 2885–2896.
- (62) Xu, L.; Møller, K. H.; Crounse, J. D.; Otkjær, R. V.; Kjaergaard, H. G.; Wennberg, P. O. Unimolecular Reactions of Peroxy Radicals Formed in the Oxidation of α-Pinene and β -Pinene by Hydroxyl Radicals. J. Phys. Chem. A 2019, 123 (8), 1661–1674.
- (63) Aschmann, S. M.; Atkinson, R. Rate Constants for the Gas-Phase Reactions of Alkanes with Cl Atoms at 296 \pm 2 K. Int. J. Chem. Kinet. 1995, 27, 613.
- (64) Vereecken, L.; Nozière, B. H Migration in Peroxy Radicals under Atmospheric Conditions. *Atmos. Chem. Phys.* 2020, 20 (12), 7429–7458.
- (65) Ziemann, P. J.; Atkinson, R. Kinetics, Products, and Mechanisms of Secondary Organic Aerosol Formation. *Chem. Soc. Rev.* 2012, 41 (19), 6582.
- (66) Rindelaub, J. D.; Borca, C. H.; Hostetler, M. A.; Slade, J. H.; Lipton, M. A.; Slipchenko, L. V.; Shepson, P. B. The Acid-Catalyzed Hydrolysis of an α-Pinene-Derived Organic Nitrate: Kinetics, Products, Reaction Mechanisms, and Atmospheric Impact. *Atmos. Chem. Phys.* 2016, 16 (23), 15425–15432.
- (67) Bean, J. K.; Hildebrandt Ruiz, L. Gas-Particle Partitioning and Hydrolysis of Organic Nitrates Formed from the Oxidation of α -

- Pinene in Environmental Chamber Experiments. Atmos. Chem. Phys. 2016, 16, 2175-2184.
- (68) Takeuchi, M.; Ng, N. L. Chemical Composition and Hydrolysis of Organic Nitrate Aerosol Formed from Hydroxyl and Nitrate Radical Oxidation of α -Pinene and β -Pinene. Atmos. Chem. Phys. 2019, 19 (19), 12749–12766.
- (69) Carter, W. P. L.; Cocker, D. R.; Fitz, D. R.; Malkina, I. L.; Bumiller, K.; Sauer, C. G.; Pisano, J. T.; Bufalino, C.; Song, C. A New Environmental Chamber for Evaluation of Gas-Phase Chemical Mechanisms and Secondary Aerosol Formation. *Atmos. Environ.* 2005, 39, 7768–7788.
- (70) Yan, C.; Nie, W.; Vogel, A. L.; Dada, L.; Lehtipalo, K.; Stolzenburg, D.; Wagner, R.; Rissanen, M. P.; Xiao, M.; Ahonen, L.; Fischer, L.; Rose, C.; Bianchi, F.; Gordon, H.; Simon, M.; Heinritzi, M.; Garmash, O.; Roldin, P.; Dias, A.; Ye, P.; Hofbauer, V.; Amorim, A.; Bauer, P. S.; Bergen, A.; Bernhammer, A.-K.; Breitenlechner, M.; Brilke, S.; Buchholz, A.; Mazon, S. B.; Canagaratna, M. R.; Chen, X.; Ding, A.; Dommen, J.; Draper, D. C.; Duplissy, J.; Frege, C.; Heyn, C.; Guida, R.; Hakala, J.; Heikkinen, L.; Hoyle, C. R.; Jokinen, T.; Kangasluoma, J.; Kirkby, J.; Kontkanen, J.; Kürten, A.; Lawler, M. J.; Mai, H.; Mathot, S.; Mauldin, R. L.; Molteni, U.; Nichman, L.; Nieminen, T.; Nowak, J.; Ojdanic, A.; Onnela, A.; Pajunoja, A.; Petäjä, T.; Piel, F.; Quéléver, L. L. J.; Sarnela, N.; Schallhart, S.; Sengupta, K.; Sipilä, M.; Tomé, A.; Tröstl, J.; Väisänen, O.; Wagner, A. C.; Ylisirniö, A.; Zha, Q.; Baltensperger, U.; Carslaw, K. S.; Curtius, J.; Flagan, R. C.; Hansel, A.; Riipinen, I.; Smith, J. N.; Virtanen, A.; Winkler, P. M.; Donahue, N. M.; Kerminen, V.-M.; Kulmala, M.; Ehn, M.; Worsnop, D. R. Size-Dependent Influence of NOx on the Growth Rates of Organic Aerosol Particles. Sci. Adv. 2020, 6 (22), eaay4945. (71) Li, Y.; Pöschl, U.; Shiraiwa, M. Molecular Corridors and Parameterizations of Volatility in the Chemical Evolution of Organic Aerosols. Atmos. Chem. Phys. 2016, 16, 3327-3344.
- (72) Booth, A. M.; Bannan, T.; McGillen, M. R.; Barley, M. H.; Topping, D. O.; McFiggans, G.; Percival, C. J. The Role of Ortho, Meta, Para Isomerism in Measured Solid State and Derived Sub-Cooled Liquid Vapour Pressures of Substituted Benzoic Acids. RSC Adv. 2012, 2 (10), 4430–4443.
- (73) Bilde, M.; Barsanti, K.; Booth, M.; Cappa, C. D.; Donahue, N. M.; Emanuelsson, E. U.; McFiggans, G.; Krieger, U. K.; Marcolli, C.; Topping, D.; Ziemann, P.; Barley, M.; Clegg, S.; Dennis-Smither, B.; Hallquist, M.; Hallquist, Å. M.; Khlystov, A.; Kulmala, M.; Mogensen, D.; Percival, C. J.; Pope, F.; Reid, J. P.; Ribeiro da Silva, M. A. V.; Rosenoern, T.; Salo, K.; Soonsin, V. P.; Yli-Juuti, T.; Prisle, N. L.; Pagels, J.; Rarey, J.; Zardini, A. A.; Riipinen, I. Saturation Vapor Pressures and Transition Enthalpies of Low-Volatility Organic Molecules of Atmospheric Relevance: From Dicarboxylic Acids to Complex Mixtures. *Chem. Rev.* 2015, 115 (10), 4115–4156.
- (74) Soonsin, V.; Zardini, A. A.; Marcolli, C.; Zuend, A.; Krieger, U. K. The Vapor Pressures and Activities of Dicarboxylic Acids Reconsidered: The Impact of the Physical State of the Aerosol. *Atmos. Chem. Phys.* 2010, 10 (23), 11753–11767.
- (75) Dang, C.; Bannan, T.; Shelley, P.; Priestley, M.; Worrall, S. D.; Waters, J.; Coe, H.; Percival, C. J.; Topping, D. The Effect of Structure and Isomerism on the Vapor Pressures of Organic Molecules and Its Potential Atmospheric Relevance. *Aerosol Sci. Technol.* 2019, 53 (9), 1040–1055.
- (76) Bannan, T. J.; Le Breton, M.; Priestley, M.; Worrall, S. D.; Bacak, A.; Marsden, N. A.; Mehra, A.; Hammes, J.; Hallquist, M.; Alfarra, M. R.; Krieger, U. K.; Reid, J. P.; Jayne, J.; Robinson, W.; McFiggans, G.; Coe, H.; Percival, C. J.; Topping, D. A Method for Extracting Calibrated Volatility Information from the FIGAERO-HR-ToF-CIMS and Its Experimental Application. *Atmos. Meas. Tech.* 2019, 12, 1429–1439.
- (77) Buchholz, A.; Ylisirniö, A.; Huang, W.; Mohr, C.; Canagaratna, M.; Worsnop, D. R.; Schobesberger, S.; Virtanen, A. Deconvolution of FIGAERO-CIMS Thermal Desorption Profiles Using Positive Matrix Factorisation to Identify Chemical and Physical Processes during Particle Evaporation. *Atmos. Chem. Phys.* 2020, 20, 7693–7716.

- (78) Huang, W.; Saathoff, H.; Pajunoja, A.; Shen, X.; Naumann, K. H.; Wagner, R.; Virtanen, A.; Leisner, T.; Mohr, C. α-Pinene Secondary Organic Aerosol at Low Temperature: Chemical Composition and Implications for Particle Viscosity. *Atmos. Chem. Phys.* 2018, 18 (4), 2883–2898.
- (79) Henry, K. M.; Lohaus, T.; Donahue, N. M. Organic Aerosol Yields from ??-Pinene Oxidation: Bridging the Gap between First-Generation Yields and Aging Chemistry. *Environ. Sci. Technol.* 2012, 46 (22), 12347–12354.
- (80) Odum, J. R.; Hoffmann, T.; Bowman, F.; Collins, D.; Flagan, R. C.; Seinfeld, J. H. Gas/Particle Partitioning and Secondary Organic Aerosol Yields. *Environ. Sci. Technol.* 1996, 30 (8), 2580–2585.
- (81) Kroll, J. H.; Seinfeld, J. H. Representation of Secondary Organic Aerosol Laboratory Chamber Data for the Interpretation of Mechanisms of Particle Growth. *Environ. Sci. Technol.* 2005, 39 (11), 4159–4165.
- (82) Cocker, D. R.; Flagan, R. C.; Seinfeld, J. H. State-of-the-Art Chamber Facility for Studying Atmospheric Aerosol Chemistry. *Environ. Sci. Technol.* 2001, 35 (12), 2594–2601.
- (83) Pathak, R. K.; Donahue, N. M.; Pandis, S. N. Ozonolysis of β -Pinene: Temperature Dependence of Secondary Organic Aerosol Mass Fraction. *Environ. Sci. Technol.* 2008, 42, 5081–5086.